ACS Energy LETTERS

http://pubs.acs.org/journal/aelccp

LETTER

Prelithiated Li-Enriched Gradient Interphase toward Practical High-Energy NMC–Silicon Full Cell

Xiaoxiao Liu,[^] Tongchao Liu,[^] Rui Wang, Zhao Cai, Wenyu Wang, Yifei Yuan, Reza Shahbazian-Yassar, Xiaocheng Li, Songru Wang, Enyuan Hu, Xiao-Qing Yang, Yinguo Xiao, Khalil Amine, Jun Lu,* and Yongming Sun*

Cite This: *ACS Energy Lett.* 2021, 6, 320–328

Read Online

ACCESS | Metrics & More | Article Recommendations | Supporting Information

ABSTRACT: It is highly desirable to realize high-energy-density lithium-ion batteries consisting of nickel-rich layered oxide cathodes (Ni-rich NMC) and Si-based anodes. A critical challenge for Ni-rich NMC is its fast capacity degradation. In addition, the low initial Coulombic efficiency of the Si-based anode consumes the electrochemically active lithium from the cathode and decreases the energy density of full batteries considerably. We consider cathode and anode as a whole to simultaneously resolve the issues of both sides. Ni-rich $LiNi_{0.65}Mn_{0.20}Co_{0.15}O_2$ (LR-Ni65) consisting of a lithium-enriched gradient interphase layer (~20 nm) is designed to supply excess electrochemically active lithium to compensate lithium loss at the anode and enhance cycling stability through regulating Li/Ni disorder in the cathode structure. We show that a LR-Ni65||Si/graphite pouch cell displays a capacity (3.29 Ah) greater than that for the counterpart using pristine Ni-rich NMC (2.95 Ah), as well as enhanced cycling stability with 88% capacity retention. The good compatibility with current Ni-rich NMC processing and facile synthesis make the as-fabricated cathode material promising for practical commercial application.

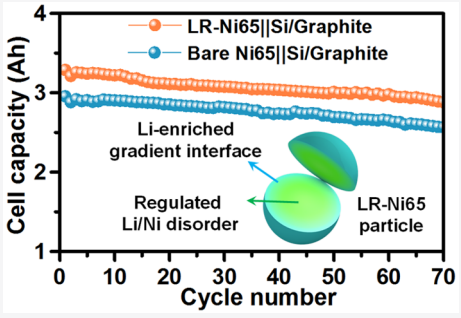

Realizing rechargeable lithium-ion batteries (LIBs) with high energy density and long service life are in high demand nowadays because of their ever-increasing applications in various fields including smart electronics, electric vehicles and cruise ships, grid-scale energy storage systems, *etc.*[1−3] While a battery is composed of multiple components, the energy density of LIBs is closely related to cell chemistry, in which electrochemically active lithium and energy output are determined by the choices of cathodes and anodes. Over the past decade, the nickel-rich layered oxide cathode ($LiNi_xMn_yCo_{1-x-y}O_2$, $x \geq 0.6$, Ni-rich NMC)|| graphite battery system has stood out from the competition and achieved great commercial success.[4−6] Although continuous efforts have pushed the currently optimal NMC cathode toward its fundamental limit of capacity, the capacity ceiling of graphite confines further improvement in the energy density of the full battery. As a result, there has been a significant push to develop the NMC cathode material with new anode chemistries. Among many promising candidates, NMC||Li metal battery with the potential to double the energy density has attracted great research interest.[7−9] However, it is still far from commercial application because of safety concerns and the underachieved cycle stability. In the near term, Ni-rich NMC||Si-based material is considered as the most viable option for next-generation battery systems, which possesses the combined advantages of high safety and reasonably high capacity in comparison to the cells with metallic Li and graphite.[10,11]

Despite anode capacity increasing with the introduction of Si, the overall performance of the current NMC||Si cells is still unsatisfactory. Si-based anode usually suffers from low initial Coulombic efficiency, which irreversibly consumes a certain amount of the lithium supply and results in a dramatic decrease in energy density.[12−14] Moreover, the high capacity of the Ni-rich cathode comes at the expense of cycle stability because of the occurrence of severe surface parasitic reactions and irreversible phase transition induced by the high Ni content.[15−18] Together, these problems have severely limited

Received: November 28, 2020
Accepted: December 22, 2020
Published: December 31, 2020

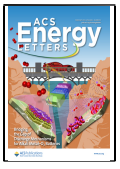

https://dx.doi.org/10.1021/acsenergylett.0c02487
ACS Energy Lett. 2021, 6, 320–328

the electrochemical properties of Ni-rich cathode. To break such limitations, enormous efforts have been separately devoted to enhancing the reversibility of Ni-rich cathodes or resolving the low Coulombic efficiency of Si anode, while rare works consider cathode and anode as a whole to improve performance. Utilizing surface engineering or morphological/compositional design, the cycle stability of Ni-rich cathodes has been significantly improved.[19−21] However, the issue of irreversible Li consumption during the first charge remains when a Ni-rich cathode is paired with a Si-based anode in full cells. Although the lithium consumption at Si-based anodes can be effectively compensated by electrochemical prelithiation and/or additive prelithiation methods,[22,23] the complicated process for electrochemical prelithiation and introduction of inert residues for additives prelithiation make them incompatible with the current battery manufacturing process. Likewise, these pretreatments show negligible effects on the cycle performance improvement of Ni-rich NMC||Si full cells. Consequently, the vast majority of research singularly contributing to Ni-rich cathode or Si-based anode shows very limited improvement in realistic NMC||Si full cells and may decelerate research innovation in meaningful directions. Li-enriched cathodes including layered oxygen cathode and spinel cathode have shown some advantages in supplying extra lithium and enhancing cycle performance, which is expected to improve the energy density and cycle life of the full battery.[24,25] However, the introduction of excess lithium without rational regulation will deteriorate the structure frame and lead to poor structure stability. This is verified by the rapid voltage decay of the Li- and Mn-rich cathode.[26] Therefore, seeking appropriate solutions to simultaneously introduce extra lithium into Ni-rich cathode materials and enhance its structural stability represents the most critical challenge for achieving high-energy-density battery systems.

In this work, we propose an innovative strategy to simultaneously resolve the issues of Ni-rich cathodes and Si anodes, realizing a realistic full battery with high energy density and long service life. By the construction of a Li-enriched gradient surface and regulation of the Li/Ni disorder of the bulk Ni-rich NMC, the as-achieved Ni-rich NMC cathode shows enhanced cycling stability and higher initial charge capacity that validly compensates lithium loss at the Si-based anode. This not only maximizes the energy density but also extends the cycle life of Ni-rich NMC||Si-based material full batteries. Gathered evidence reveals that the reconstructed Li-enriched gradient surface can release the prestored additional Li to effectively compensate for the initial lithium loss at the Si-based anodes. Meanwhile, the induced Li/Ni disorder of the bulk is beneficial to enhance the structural stability for long-term cycling of the Ni-rich NMC cathode. As a result, the elaborately designed Li-enriched $LiNi_{0.65}Mn_{0.20}Co_{0.15}O_2$ (LR-Ni65) exhibits a charge specific capacity that is 24 mAh g^{-1} greater than that of the pristine Ni65 (220 mAh g^{-1} vs 196 mAh g^{-1}) and improved cycle stability. More importantly, to demonstrate the practicality of this modification, we fabricated 3 Ah Ni-rich||Si/graphite pouch cells that exhibit an energy density increase of 11% to 427 Wh kg^{-1} (calculated based on active materials of cathode and anode), which represents a significant breakthrough in realistic batteries. This study opens new space for the performance improvement of a practical battery and pioneers a new research direction that comprehensively focuses on cathode stability and the Li consumption cycle of the anode.

The typical Ni-rich cathode $[Li(Ni_xMn_yCo_{1-x-y})O_2]$ materials adopt the α-$NaFeO_2$ type layered structure and consist of alternating layers of Li ions and transition-metal ions separated by oxygen atomic layers.[27] Excess Li could be stored at the surface or in the bulk because of the open structural framework to form $Li_{1+\delta}(Ni_xMn_yCo_{1-x-y})O_2$ without causing bond breakage and the collapse of the overall structure.[28] Meanwhile, the excess Li storage requires the cooperation of active transition metals (TMs) that have an accessible lower oxidation state. Fundamentally, the reducibility of TMs is determined by their chemical states and the corresponding electronic structures. In Ni-rich NMC cathodes, Ni^{3+} (with an electronic configuration of $t_{2g}^6e_g^1$) coexists with Ni^{2+} ($t_{2g}^6e_g^2$), while Co^{3+} and Mn^{4+} exist individually without any other oxidation states.[5] As shown in Figure 1a, it is clear that the reduction of Ni^{3+} to Ni^{2+}

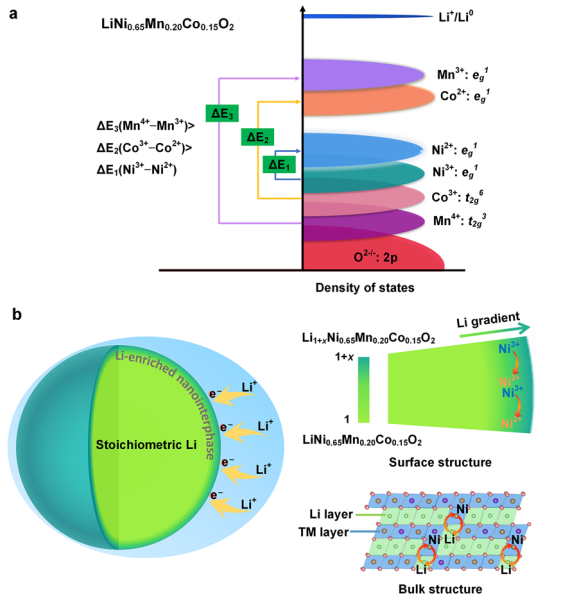

Figure 1. Li-enriched gradient NMC cathode materials design and fabrication. (a) Redox behaviors of transition-metal cations (Ni, Mn, and Co) and oxygen anions of the $LiNi_{0.65}Mn_{0.20}Co_{0.15}O_2$ cathode. (b) Schematic illustration of the topotactic chemical reaction process (left), the formed lithium enriched gradient interphase structure (top right, surface structure), and the bulk structure of $LiNi_{0.65}Mn_{0.20}Co_{0.15}O_2$ cathode with partial Li/Ni disorder (bottom right, bulk structure).

preferentially occurs because of the lower energy barriers compared with the redox of $Mn^{4+/3+}$ and $Co^{3+/2+}$ ($E_1 < E_2 < E_3$).[29] Although having a negligible effect on the structure framework, the presence of high Ni^{2+} content may cause the evolution of local structure. Because of the similar ionic radius of Li^+ (0.76 Å) with Ni^{2+} (0.69 Å) and oxygen deficiency during the sintering process, Ni^{2+} ions can migrate to the lithium octahedral 3a sites leading to Li/Ni exchange,[15,30,31] which has been considered to have a significant impact on the electrochemical performance of the Ni-rich cathode. The appropriate content of Li/Ni disorder can improve the structural stability of cathode materials benefiting from the electrochemically inactive Ni^{2+} in 3a sites serving as the structural stabilizer, but too much Li/Ni antisite would reduce capacity significantly because of the hindrance of antisite Ni in Li-ion diffusion pathways.[4,32,33] Therefore, the simultaneous achievements of excess Li storage and the rational regulation of

https://dx.doi.org/10.1021/acsenergylett.0c02487
ACS Energy Lett. 2021, 6, 320−328

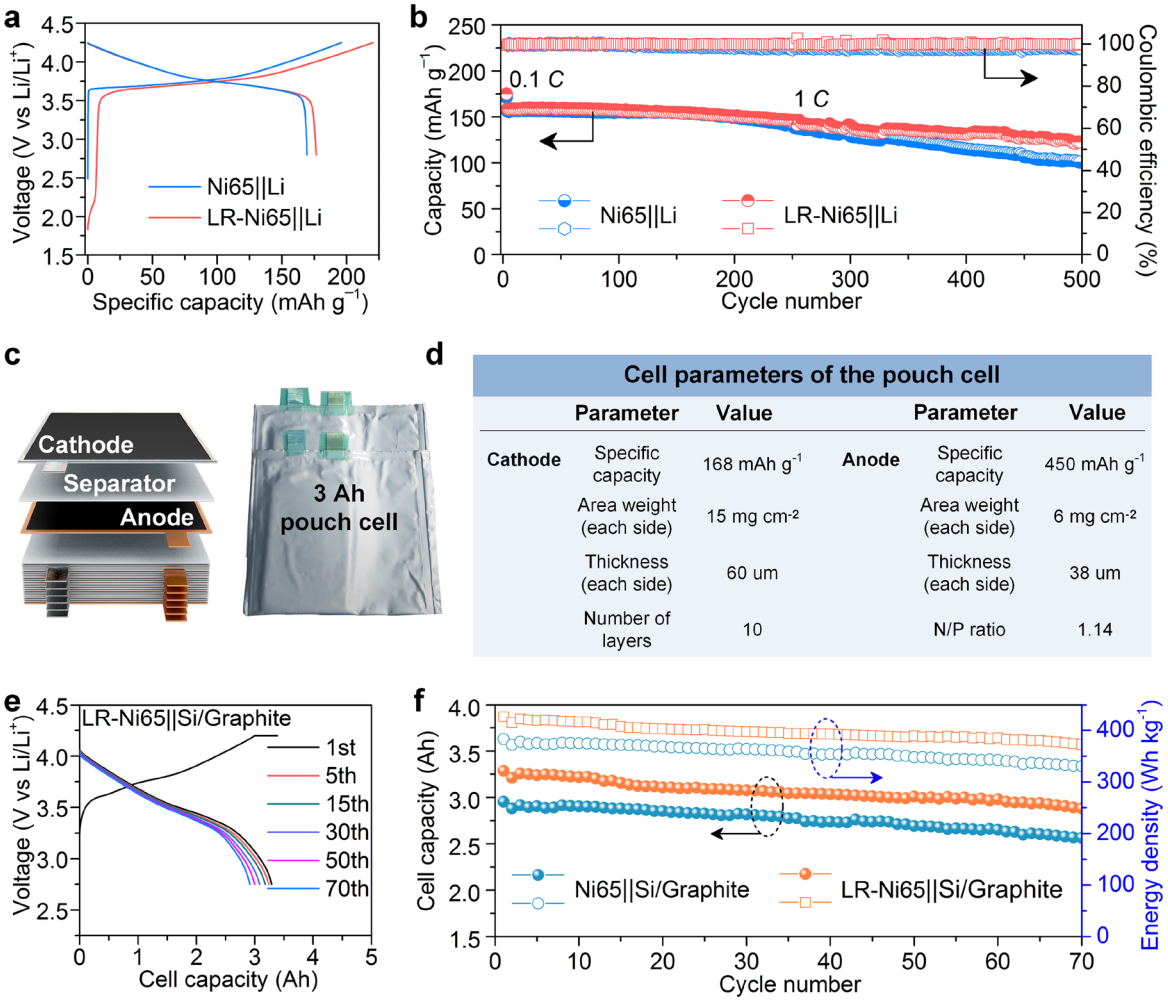

Figure 2. Electrochemical performances of pristine and LR-Ni65 cathodes in half cells and pouch cells. (a) The comparison of initial capacity−voltage curves and (b) cycling performance for the Ni65 and LR-Ni65 electrodes in half cells. (c) Configuration of the fabricated pouch cells with stacked structures and (d) parameters of the pouch cells. The specific capacity of cathode and anode as well as the N/P capacity ratio is obtained based on the current density at 0.5C. (e) Cell voltage−capacity profiles of LR-Ni65||Si/graphite pouch cell. (f) Cycling performances of LR-Ni65||Si/graphite and Ni65||Si/graphite pouch cells. Energy density was calculated based on active material mass loading of anode and cathode.

Li/Ni disorder are highly desirable but represent a critical challenge.

Here, we employed a Ni-rich cathode $LiNi_{0.65}Mn_{0.20}Co_{0.15}O_2$ (Ni65) as a model system and conducted a facile topotactic chemical reaction to realize the goals of introducing and storing excess lithium and simultaneously regulating the Li/Ni disorder to maximize the energy density and improve the cycle stability of Ni65||Si/graphite full batteries. The topotactic chemical reaction process was performed in the Ar atmosphere using a lithium complex solution ($C_{10}H_8Li$ in tetrahydrofuran) as the reaction chemical reagent with the chemical reaction equation $LiNi_{0.65}Mn_{0.20}Co_{0.15}O_2 + xC_{10}H_8Li \rightarrow Li_{1+x}Ni_{0.65}Mn_{0.20}Co_{0.15}O_2 + C_{10}H_8$ (Figures S1 and S2). Only active lithium was introduced into the Ni65 to form LR-Ni65 material through such a chemical reaction process. Because of the high reducibility of Naph-Li,[34−36] the Ni^{3+} on the surface of Ni65 would first be reduced to Ni^{2+}, accompanied by inserting Li^+ into Ni65. Thus, a lithium- and Ni^{2+}-rich surface layer could be constructed, as illustrated in Figure 1b. More Ni^{2+} would increase Li/Ni exchange of the bulk material, which can stabilize the structure of LR-Ni65.

The electrochemical properties of the pristine Ni65 and LR-Ni65 materials were first compared by the galvanostatic charge−discharge technique in the potential range of 2.8−4.25 V in half cells. The initial capacity−voltage curves and the corresponding differential capacity versus voltage (dQ/dV) profiles of the Ni65 and LR-Ni65 electrodes are shown in Figures 2a and S3, respectively. Different from the pristine Ni65 electrode, a distinct additional charge voltage plateau was observed around 2.0 V for the LR-N65 electrode, indicating the extraction of excess lithium from the LR-Ni65. This feature was further verified by the cyclic voltammograms that indicate a new oxidation peak was observed in this voltage range of the LR-Ni65 electrode (Figure S4). This voltage plateau or oxidation peak indicated the successful introduction of electrochemically active lithium into the LR-Ni65 structure.[37] Benefiting from the electrochemical extraction of excess lithium prestored during the chemical treatment process, the overall voltage−capacity curve of the LR-Ni65 electrode shifted right and showed a high initial charge capacity of 220 mAh g^{-1}, which was 24 mAh g^{-1} greater than that of the pristine Ni65 electrode (196 mAh g^{-1}). The extra charge capacity is specially designed to supplement irreversible Li

https://dx.doi.org/10.1021/acsenergylett.0c02487
ACS Energy Lett. 2021, 6, 320−328

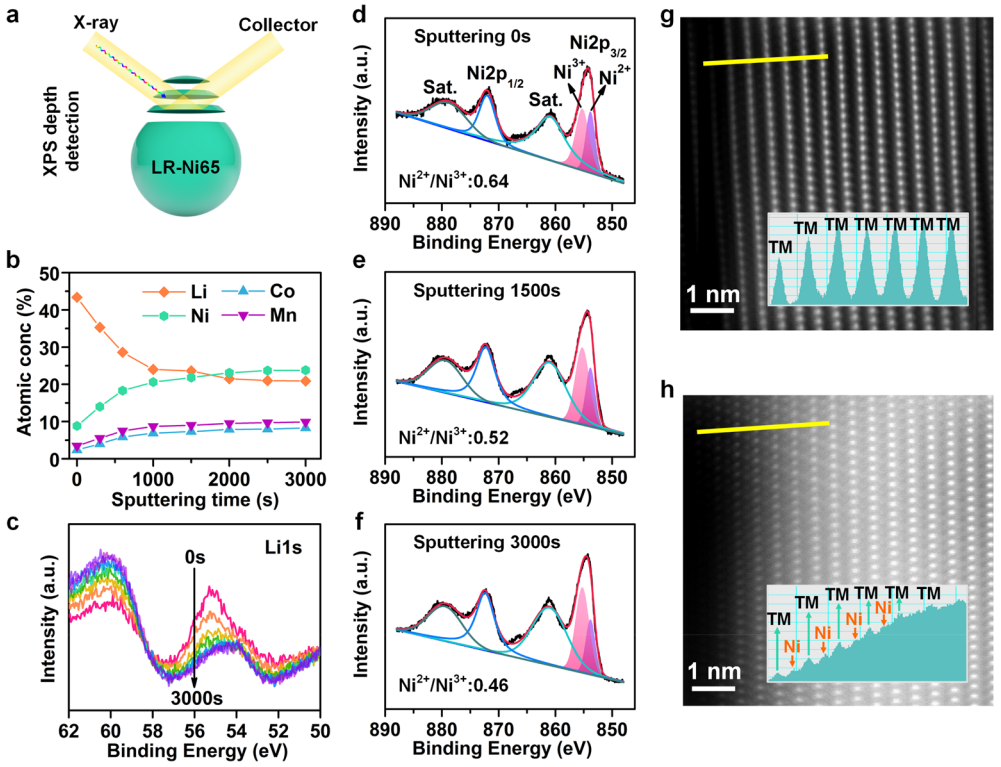

Figure 3. Surface characterizations of the LR-Ni65 cathodes. (a) Schematic illustration of XPS depth detection for LR-Ni65 particles with Ar sputtering. (b) Element atomic concentrations of Li, Ni, Mn, and Co in LR-Ni65 obtained from XPS results. (c) High-resolution XPS results of Li 1s spectra for LR-Ni65 with different sputtering time cycles. (d–f) High-resolution XPS spectra of Ni 2p for LR-Ni65 with different sputtering times. Scanning transition electron microscopy (STEM) image of Ni65 (g) and (h) LR-Ni65 and the corresponding interplanar spacing profiles.

consumption of the Si anode during the first charge. The discharge capacity of the LR-Ni65 electrode was 177 mAh g^{-1}, which was greater than that of the pristine Ni65 electrode (169 mAh g^{-1}) as well. The possible reason for the higher discharge capacity is that topotactic chemical preinserted lithium can minimize off-stoichiometry and compensate for the electrochemical active Li vacancies of Ni65, which are usually generated during the high-temperature materials' synthesis procedure.[38,39]

Cycling stability of two comparable samples was further evaluated in half cells (Figure 2b). The LR-Ni65 electrode displayed high capacity retentions of 88.7% for 300 cycles and 82.6% for 400 cycles at 1C (Figure S5). In contrast, the capacity retentions of the pristine Ni65 electrode were 82.7% for 300 cycles and 73.8% for 400 cycles. Even after 500 cycles, the LR-Ni65 electrode still delivered a specific capacity of 125 mAh g^{-1} with 77.3% capacity retention. This was significantly greater than 98 mAh g^{-1} with 64.3% capacity retention for the pristine Ni65 electrode. Panels a and b of Figure S6 show the charge–discharge curves of the pristine Ni65 and LR-Ni65 electrodes for the first and 500th cycles at a current density of 1C, respectively. The LR-Ni65 electrode displayed much lower overpotential and higher specific capacity than the pristine Ni65 electrode after 500 cycles at 1C. Note that capacity degradation of layered Ni-rich NMC cathodes is a critical barrier hindering their commercialization. Interestingly, we find that the topotactic chemical treatment can dramatically enhance the capacity retention and voltage stability of the LR-Ni65 electrode. In addition, the LR-Ni65 also shows good environmental stability which is of vital importance for industrial application. After the exposure of the LR-Ni65 in dry air for 3 h, a high initial charge specific capacity of 215 mAh g^{-1} was achieved, which was very close to the value of fresh LR-Ni65 (Figure S7). Even after exposure in ambient air with 30% humidity for 3 h, the LR-Ni65 still delivered an initial charge capacity of 204 mAh g^{-1}, which is 8 mAh g^{-1} greater than that of the pristine Ni65 without exposure. Note that Ni-rich NMC cathode materials are highly air-sensitive and need to be processed in a dry room with low dew-point temperature in the battery industry. Regarding this aspect, the obtained LR-Ni65 can be well compatible with the industrial Ni-rich NMC cathode-processing process.

All the above features of better capacity retention, higher discharge working voltage, and higher discharge specific capacity make the LR-Ni65 electrode an ideal cathode for high-energy-density LIBs using high-capacity Si-based or other anodes that have high specific capacities but relatively low initial Coulombic efficiency (ICE) because of the severe parasitic reactions. The extra lithium donation from LR-Ni65 in the initial charge process can compensate for lithium loss on such anodes and improve the energy density of batteries. To elucidate the positive effect in improving the energy density of full cells using this LR-Ni65 cathode, we fabricated 3 Ah class pouch-type full cells using LR-Ni65 as the cathode pairing with Si/graphite anode (LR-Ni65||Si/graphite) on commercialized battery active materials mass loading. The pristine Ni65||Si/graphite cell was used as the contrast. The pouch-type full cells were constructed by stacking layers of cathode, separator, and anode (Figure 2c). The detailed parameters of fabricated pouch cells are listed in Figure 2d. As shown in Figures 2e and S8, because of the compensation of lithium loss for the Si/graphite anode from extra preintroduced lithium in the LR-

https://dx.doi.org/10.1021/acsenergylett.0c02487
ACS Energy Lett. 2021, 6, 320–328

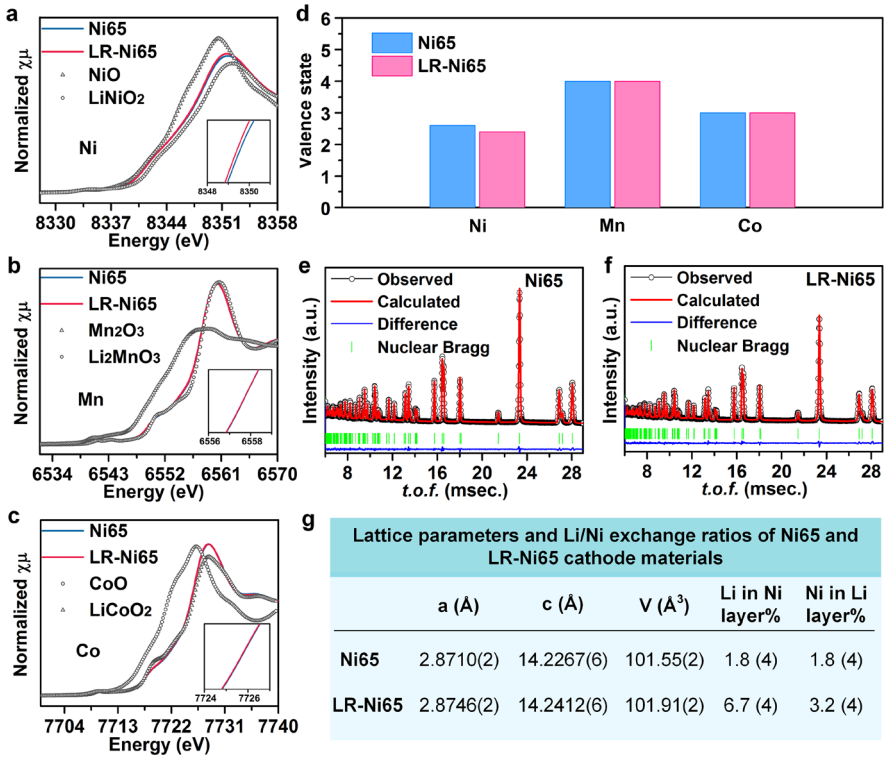

g

Lattice parameters and Li/Ni exchange ratios of Ni65 and LR-Ni65 cathode materials

	a (Å)	c (Å)	V (Å^3)	Li in Ni layer%	Ni in Li layer%
Ni65	2.8710(2)	14.2267(6)	101.55(2)	1.8 (4)	1.8 (4)
LR-Ni65	2.8746(2)	14.2412(6)	101.91(2)	6.7 (4)	3.2 (4)

Figure 4. Comparison of bulk structures between the pristine Ni65 and LR-Ni65 cathodes. X-ray absorption near-edge spectra for (a) Ni, (b) Mn, and (c) Co K-edges (inset: zoomed-in view in the selected energy ranges). (d) Valence states of individual elements (Ni, Mn, and Co) in Ni65 and LR-Ni65 materials. Refined neutron powder diffraction (NPD) patterns of the (e) Ni65 and (f) LR-Ni65 materials. (g) Lattice parameters and Li/Ni exchange ratios of Ni65 and LR-Ni65 materials.

Ni65 cathode, the LR-Ni65||Si/graphite cell displayed higher reversible discharge capacities than the Ni65||Si/graphite cell at 0.2*C*. An 11% energy density increase was achieved for the LR-Ni65||Si/graphite full cell (427 vs 383 Wh kg^{-1}) for the first discharge process. As revealed in Figure 2f, even after 70 cycles, the LR-Ni65||Si/graphite full cell still displayed a capacity that was 0.32 Ah higher than that of the pristine Ni65|| Si/graphite cell (2.88 vs 2.56 Ah, corresponding to 373 vs 330 Wh kg^{-1}). Besides, no apparent bulges were observed for both pouch cells after cycling, indicating that the lithium preintercalation process does not pose negative effects on the detrimental gas generation of full cells (Figure S9).

The above promising electrochemical data has motivated us to investigate the microstructure and composition of the as-achieved Ni65 materials, and uncover the relationship between the structure, composition and properties. The chemical lithium intercalation penetrates into the surface of the Ni65 materials. Thus, the surface layer of LR-Ni65 has a higher content of lithium and Ni^{2+} than the inner, and the change of Li/Ni disorder predominantly takes place on the surface, leading to the formation of a reconstruction surface layer. X-ray photoelectron spectroscopy (XPS) depth test was conducted to investigate the reconstruction of the surface structure of LR-Ni65 (Figure 3a). The XPS depth profiles for LR-N65 were obtained with different sputtering time cycles under argon plasma. Figure 3b showed the plots of atomic concentration (Li, Ni, Co, and Mn) and sputtering time. With the increase of sputtering time, the Li 1s signal in the high-resolution XPS spectra dropped gradually and then stayed stable after a sputtering time of 2500 s (Figure 3c), and the calculated Li concentration changed accordingly, which indicated the gradient distribution of lithium element in the lithium-enriched surface layer. The outer surface had double value in the calculated Li concentration in comparison to the inner part. High-resolution Ni 2p XPS results demonstrated that the Ni^{2+}/Ni^{3+} ratio decreased from 0.64 to 0.46 over the sputtering time from 0 to 2500 s, and it kept constant in the following test time (Figures 3d–f and S10). The oxidation states of Mn and Co stayed unchanged during all the measured time, suggesting that these two elements were not reduced during the fabrication of LR-Ni65 (Figure S11). This gradient lithium-enriched surface layer was about 20 nm based on the XPS depth measurement with V_2O_5 as the reference sample. Scanning transition electron microscopy (STEM) was further conducted to characterize the atomic structure of the samples (Figure 3g,h). No Li/Ni disorder was detected for Ni65, while, as expected, Li/Ni disorder was clearly observed on the surface layer of LR-Ni65. Surface structure with a higher content of Ni^{2+} may effectively suppress the irreversible phase transition from the layer structure to rack-salt NiO and be beneficial for improving the cycling stability.

The chemical lithium intercalation processing also regulated the bulk structure of the Ni65 materials. Considering the greatly enhanced structural stability and improved electrochemical performance, two key issues should be considered further: (1) How does the structure of Ni65 evolve during the chemical treatment? (2) What effects does this regulated structure have on the electrochemical performance of LR-Ni65? To fully understand the structural change of the bulk of LR-Ni65, we further employed a concerted investigation using X-ray absorption spectroscopy (XAS), neutron powder diffraction (NPD), *ex situ* and *in situ* X-ray powder-diffraction (XRD), and Rietveld refinements to quantitatively investigate the structure discrepancy between Ni65 and LR-Ni65. X-ray

https://dx.doi.org/10.1021/acsenergylett.0c02487
ACS Energy Lett. 2021, 6, 320−328

absorption near-edge spectroscopy (XANES) was carried out to examine the valence states of Ni, Mn, and Co elements and their local environment in the cathode materials (Figure 4a–c). In comparison with Ni65, the edge of the Ni K-edge spectra of LR-Ni65 shifted to a lower energy, suggesting a decreased average valence state of Ni. The Mn and Co K-edges remained constant, which is consistent with the expected results based on the reduction energies of metal elements (Figure 1a). The fitting results show that the average valence state of Ni in Ni65 was 2.6 and in LR-Ni65 was 2.4 (Figures 4d and S12), suggesting that some Ni^{3+} was reduced to Ni^{2+} during the fabrication of LR-Ni65. Fourier transformation (FT) of EXAFS spectra was used to characterize the local bond length of Ni, Mn, and Co transition metals in cathode materials (Figure S13). With excess lithium intercalation into the structure of LR-Ni65, the bond lengths of both Mn–O and Co–O in LR-Ni65 showed negligible change (both are around 1.4 Å) in comparison to Ni65, suggesting the valence state of Mn^{4+} and Co^{3+} remain constant throughout the chemical reaction.[40] However, the Ni–O bond exhibited small fluctuations in peak intensity, which was caused by the variation in the relative concentration of Ni^{2+}/Ni^{3+}. The height of the shoulder peak at 1.5 Å (corresponding to Ni^{3+}–O bond length) decreased, while the height of the shoulder peak at 1.7 Å (corresponding to Ni^{2+}–O bond length) increased. This outcome suggests the increase of Ni^{2+} and decrease of Ni^{3+} content in LR-Ni65 cathode materials.[30,41]

The corresponding NPD patterns and the deduced structural parameters of the Ni65 and LR-Ni65 samples are shown in Figure 4e–g. Although they both exhibited the characteristic peaks for a well-crystallized layered hexagonal a-$NaFeO_2$ structure with $R\bar{3}m$ symmetry, some difference in microstructure (cell parameters and atomic occupancies) was detected by Rietveld refinement using the FULLPROF program. As shown in Figure 4g, the refinement results show that both lattice parameters a and c of LR-Ni65 exhibited a slight increase compared with Ni-65. The expansion of the lattice parameter a can be attributed to the reduction of Ni from Ni^{3+} to Ni^{2+}, while the increase in lattice parameter c might result from the Li insertion into the defect position in the structure of the initial Ni65.[32] More interestingly, we observed a slight increase in Li/Ni disorder after the topotactic chemical treatment. It is worth noting that Li/Ni disorder, a common structural defect in Ni-rich NMC cathode, is crucially important for electrochemical performance.[33,42] Ni^{2+} has been previously proven to be the dominant cationic ion participating in Li/Ni disorder because of a combination of their similar ion radius, magnetic frustration of transition-metal layer, and superexchange interactions.[4,15] Accordingly, the increase in Li/Ni disorder of LR-Ni65 is directly associated with the reduction of Ni^{3+} that occurs in the topotactic chemical reaction process. The appearance of Li/Ni disorder will relieve magnetic frustration and improve the structural stability of Ni-rich NMC materials benefiting from the electrochemically inactive Ni^{2+} in 3a sites serving as the structural stabilizer. On the other hand, too much Li/Ni disorder may hinder the transmission pathway of Li^+.[43,44] Figure S14 shows that the rate performance of LR-Ni65 is not affected by the increased Li/Ni disorder, indicating the suitable degree of Li/Ni disorder.

Operando XRD was carried out to directly monitor the cathode structural evolution with a model system of electrochemical lithium intercalation method. The *in situ* XRD results of electrochemical lithium intercalation into Ni65 are shown in Figure S15. During the lithiation process of Ni65, a voltage plateau for lithium intercalation around 1.7 V was observed, corresponding to the lithium extraction plateau around 2.0 V for LR-Ni65 (Figure 2a). It is noted that this voltage plateau extended to a high lithium-ion capacity over 150 mAh g^{-1} (stage I to II in Figure S15), while the intensity and position of the (003) peak in the XRD pattern remained almost constant, which indicated that the overall structure of Ni65 remained unchanged during such an amount of lithium insertion. Thus, lithium-ion capacity greater than 25 mAh g^{-1} (the typical sample LR-Ni65) could be inserted into the structure. Experimentally, we showed that the electrochemical insertion of different lithium ion capacities from 20 to 60 mAh g^{-1} into Ni65 was successfully realized, and these lithium ions were extracted reversibly during the initial charging process (Figure S16a). Meanwhile, the preinsertion of these lithium ions did not show any negative effect on the following electrochemical cycling of these materials (Figure S16). Therefore, the amount of introduced excess lithium in LR-Ni65 can be adjusted to pair with anodes with different Coulumbic efficiency in full batteries to compensate for the lithium loss and maximize the energy density of batteries. Overlithiation of Ni65 with the capacity greater than 200 mAh g^{-1} would finally lead to the degradation of the crystal structure.

The morphology and crystal structure of the Ni65 and LR-Ni65 after cycles were also characterized by scanning electron microscopy (SEM) and XRD. SEM images show that both the Ni65 and LR-Ni65 electrodes maintained their original morphology that micrometer-sized secondary particles remained homogeneously distributed in the electrodes without generating cracks (Figure S17). After 500 cycles, the XRD pattern of the LR-Ni65 electrode displayed clear splitting of (006)/(102) and (108)/(110) peaks, indicating the initial phase structure of layered hexagonal a-$NaFeO_2$ well remained (Figure S18). In contrast, LR-Ni65 exhibited a higher peak intensity ratio for (003)/(104) than the pristine Ni65 electrode after cycling, which suggested the good structure stability of LR-Ni65 and thus explained their long-term cycling performance. Electrochemical impedance spectroscopy (EIS) measurements were also carried out for Ni65 and LR-Ni65 electrodes after the 1st, 100th, and 250th cycles (Figure S19). The surface charge-transfer resistance (R_{ct}) of both electrodes were similar after the first charge–discharge cycle. The R_{ct} of Ni65 electrode decreased from 54 to 26 Ω from the 1st to the 100th cycles and then increased to 65 Ω at the 250th cycle. The LR-Ni65 Ni65 electrodes showed similar variations in R_{ct}. The values of R_{ct} and overall impedance of LR-Ni65 were much lower than that of the Ni65 electrode after 250 cycles, again supporting the good stability of the LR-Ni65 electrode.

The topotactic chemical lithium intercalation can also be generalized to other Ni-based metal oxide cathodes with mixed valence state of Ni (II and III) and improve the electrochemical performance. Here, we take NMC532 (namely Ni50 in the following discussion) cathode material as another sample. As shown in Figure S20, Ni50 electrode after lithium preintercalation (LR-Ni50) by topotactic chemical reaction exhibited lower initial open-circuit voltages and different potential profiles during the first-cycle charging process in comparison to the corresponding pristine electrode. A new voltage plateau appeared around 2.0 V during the charge process. The voltage plateau was caused by the chemical lithium insertion process and can contribute extra lithium-ion

https://dx.doi.org/10.1021/acsenergylett.0c02487
ACS Energy Lett. 2021, 6, 320–328

capacities during the first-cycle charge process. As expected, a higher overall initial charge capacity of 21 mAh g^{-1} was achieved for the LR-Ni50 in comparison to its counterpart (202 mAh g^{-1} for LR-Ni50 vs 181 mAh g^{-1} for the pristine Ni50). Meanwhile, the discharge capacities of the LR-Ni50 was slightly higher than the pristine Ni50. Stable cycling was also achieved for the LR-Ni50.

In summary, we demonstrate an innovative surficial Li concentration-gradient NMC material with slight bulk Li/Ni disorder (LR-Ni65) to simultaneously resolve the issues of structural stability for Ni-rich cathodes and lithium loss for Si anodes, realizing a realistic Ah-class pouch-type NMC||Si/graphite full battery with 11% increase in energy density in comparison to the counterpart with pristine NMC cathode, as well as long service life. Detailed structural and chemical analysis characterized by depth XPS, HRTEM, XAS, NPD, *in situ* XRD *etc.* revealed that the dramatically improved electrochemical performance of LR-Ni65 was associated with the reconstruction of surface structure and regulated Li/Ni disorder. The slightly increased Li/Ni disorder can help to stabilize the structure of LR-Ni65 during cycling. The lithium-enriched gradient surface layer can donate excess lithium ions in the first charge process, compensating lithium loss at Si/graphite anodes and increasing the energy density of LIBs. The present work will be instructive for the design of an advanced full-cell with high energy density and extended cycle life via NMC cathode material Li/Ni disorder engineering and surface reconstruction and may accelerate the extensive commercialization of Si-based anodes in electric vehicles.

■ ASSOCIATED CONTENT

Supporting Information

The Supporting Information is available free of charge at https://pubs.acs.org/doi/10.1021/acsenergylett.0c02487.

Detailed information on material and electrochemical measurement, X-ray absorption spectroscopy tests, neutron and X-ray diffraction tests, scanning electron microscopy, transmission electron microscopy, Raman spectrometry, and X-ray photoelectron spectroscopy measurements; further electrochemical characteristics and Raman, XPS, XAS, SEM, and TEM results are also provided (PDF)

■ AUTHOR INFORMATION

Corresponding Authors

Jun Lu − *Chemical Sciences and Engineering Division, Argonne National Laboratory, Lemont, Illinois 60439, United States;* orcid.org/0000-0003-0858-8577; Email: junlu@anl.gov

Yongming Sun − *Wuhan National Laboratory for Optoelectronics, Huazhong University of Science and Technology, Wuhan 430074, China;* orcid.org/0000-0001-8528-525X; Email: yongmingsun@hust.edu.cn

Authors

Xiaoxiao Liu − *Wuhan National Laboratory for Optoelectronics, Huazhong University of Science and Technology, Wuhan 430074, China*

Tongchao Liu − *Chemical Sciences and Engineering Division, Argonne National Laboratory, Lemont, Illinois 60439, United States*

Rui Wang − *School of Advanced Materials, Peking University, Shenzhen Graduate School, Shenzhen 518055, China*

Zhao Cai − *Wuhan National Laboratory for Optoelectronics, Huazhong University of Science and Technology, Wuhan 430074, China;* orcid.org/0000-0001-7110-9300

Wenyu Wang − *Wuhan National Laboratory for Optoelectronics, Huazhong University of Science and Technology, Wuhan 430074, China*

Yifei Yuan − *Department of Mechanical and Industrial Engineering, University of Illinois at Chicago, Chicago, Illinois 60607, United States*

Reza Shahbazian-Yassar − *Department of Mechanical and Industrial Engineering, University of Illinois at Chicago, Chicago, Illinois 60607, United States;* orcid.org/0000-0002-7744-4780

Xiaocheng Li − *China Electronic New Energy Research Institute Co., Ltd., Wuhan 430074, China*

Songru Wang − *China Electronic New Energy Research Institute Co., Ltd., Wuhan 430074, China*

Enyuan Hu − *Chemistry Division, Brookhaven National Laboratory, Upton, New York 11973, United States;* orcid.org/0000-0002-1881-4534

Xiao-Qing Yang − *Chemistry Division, Brookhaven National Laboratory, Upton, New York 11973, United States;* orcid.org/0000-0002-3625-3478

Yinguo Xiao − *School of Advanced Materials, Peking University, Shenzhen Graduate School, Shenzhen 518055, China*

Khalil Amine − *Chemical Sciences and Engineering Division, Argonne National Laboratory, Lemont, Illinois 60439, United States;* orcid.org/0000-0001-9206-3719

Complete contact information is available at: https://pubs.acs.org/10.1021/acsenergylett.0c02487

Author Contributions

^X.L. and T.L. contributed equally to this work. X.L. and T.L. conceived the idea and designed the experiments. X.L. and R.W. carried out the *in situ* XRD results. Z.C., E.H., and X.Y. performed and analyzed the synchrotron-XAS. R.W. and Y.X. carried out the neutron diffraction tests and made Rietveld refinement of the cathodes' crystal structures. X.L. and S.W. conducted the commercial-level electrode and pouch full cell fabrication and measured the pouch cells' electrochemical performances. X.L. carried out the coin cells' electrochemical measurements and analysis. Y.Y. and R.S.-Y. conducted TEM measurements. X.L., T.L., J.L., Y.S., and K.A. wrote the manuscript and all authors edited the manuscript.

Notes

The authors declare no competing financial interest.

■ ACKNOWLEDGMENTS

This work is financially supported by the Natural Science Foundation of China (Grant Nos. 52072137, 52002136, and 51802105) and China Postdoctoral Science Foundation (Grant Nos. 2020T130216 and 2018M642833). The authors also gratefully acknowledge support from the U.S. Department of Energy (DOE), Office of Energy Efficiency and Renewable Energy, Vehicle Technologies Office under Clean Vehicles, US-China Clean Energy Research Centre (CERC-CVC2). Argonne National Laboratory is operated for DOE Office of Science by UChicago Argonne, LLC, under contract number DE-AC02-06CH11357. This research used resources 7-BM of the National Synchrotron Light Source II, a U.S. Department of Energy (DOE) Office of Science User Facility operated for

the DOE Office of Science by Brookhaven National Laboratory under Contract No. DE-SC0012704. E.H. and X.-Q.Y. are supported by the U.S. Department of Energy, the Assistant Secretary for Energy Efficiency and Renewable Energy, Office of Vehicle Technologies, through Advanced Battery Material Research (BMR) program under Contract Number DE-SC0012704. The research is also financially supported by Guangdong Basic and Applied Basic Research Foundation (Nos. 2019A1515012060 and 2019B1515120028). The authors acknowledge Lunhua He, Jie Chen, and Sihao Deng for their help on the experiments at GPPD in China Spallation Neutron Source (CSNS). This work made use of instruments in the Electron Microscopy Service (Research Resources Center, UIC). R.S.-Y. acknowledges the financial support from National Science Foundation Award CBET-1805938. The authors also thank the Analytical and Testing Center of Huazhong University of Science and Technology (HUST) as well as the Center for Nanoscale Characterization & Devices of Wuhan National Laboratory for Optoelectronics (WNLO) for providing the facilities to conduct the characterizations.

REFERENCES

(1) Li, M.; Liu, T.; Bi, X.; Chen, Z.; Amine, K.; Zhong, C.; Lu, J. Cationic and anionic redox in lithium-ion based batteries. *Chem. Soc. Rev.* **2020**, *49* (6), 1688−1705.

(2) Xie, J.; Lu, Y. C. A retrospective on lithium-ion batteries. *Nat. Commun.* **2020**, *11* (1), 2499.

(3) Chen, S.; Dai, F.; Cai, M. Opportunities and Challenges of High-Energy Lithium Metal Batteries for Electric Vehicle Applications. *ACS Energy Lett.* **2020**, *5* (10), 3140−3151.

(4) Yang, L.; Yang, K.; Zheng, J.; Xu, K.; Amine, K.; Pan, F. Harnessing the surface structure to enable high-performance cathode materials for lithium-ion batteries. *Chem. Soc. Rev.* **2020**, *49* (14), 4667−4680.

(5) Liu, L. H.; Li, M. C.; Chu, L. H.; Jiang, B.; Lin, R. X.; Zhu, X. P.; Cao, G. Z. Layered ternary metal oxides: Performance degradation mechanisms as cathodes, and design strategies for high-performance batteries. *Prog. Mater. Sci.* **2020**, *111*, 100655.

(6) Li, W.; Erickson, E. M.; Manthiram, A. High-nickel layered oxide cathodes for lithium-based automotive batteries. *Nat. Energy* **2020**, *5* (1), 26−34.

(7) Han, B.; Xu, D.; Chi, S. S.; He, D.; Zhang, Z.; Du, L.; Gu, M.; Wang, C.; Meng, H.; Xu, K.; Zheng, Z.; Deng, Y. 500 Wh kg^{-1} Class Li Metal Battery Enabled by a Self-Organized Core-Shell Composite Anode. *Adv. Mater.* **2020**, *32* (42), No. 2004793.

(8) Wang, E.; Dey, S.; Liu, T.; Menkin, S.; Grey, C. P. Effects of Atmospheric Gases on Li Metal Cyclability and Solid-Electrolyte Interphase Formation. *ACS Energy Lett.* **2020**, *5* (4), 1088−1094.

(9) Wang, J.; Huang, W.; Pei, A.; Li, Y.; Shi, F.; Yu, X.; Cui, Y. Improving cyclability of Li metal batteries at elevated temperatures and its origin revealed by cryo-electron microscopy. *Nat. Energy* **2019**, *4* (8), 664−670.

(10) Song, M.-S.; Chang, G.; Jung, D.-W.; Kwon, M.-S.; Li, P.; Ku, J.-H.; Choi, J.-M.; Zhang, K.; Yi, G.-R.; Cui, Y.; Park, J. H. Strategy for Boosting Li-Ion Current in Silicon Nanoparticles. *ACS Energy Lett.* **2018**, *3* (9), 2252−2258.

(11) Liu, N.; Lu, Z.; Zhao, J.; McDowell, M. T.; Lee, H. W.; Zhao, W.; Cui, Y. A pomegranate-inspired nanoscale design for large-volume-change lithium battery anodes. *Nat. Nanotechnol.* **2014**, *9* (3), 187−192.

(12) Zhao, J.; Lu, Z.; Wang, H.; Liu, W.; Lee, H. W.; Yan, K.; Zhuo, D.; Lin, D.; Liu, N.; Cui, Y. Artificial Solid Electrolyte Interphase-Protected LixSi Nanoparticles: An Efficient and Stable Prelithiation Reagent for Lithium-Ion Batteries. *J. Am. Chem. Soc.* **2015**, *137* (26), 8372−8375.

(13) Chen, S.; Niu, C.; Lee, H.; Li, Q.; Yu, L.; Xu, W.; Zhang, J.-G.; Dufek, E. J.; Whittingham, M. S.; Meng, S.; Xiao, J.; Liu, J. Critical Parameters for Evaluating Coin Cells and Pouch Cells of Rechargeable Li-Metal Batteries. *Joule* **2019**, *3* (4), 1094−1105.

(14) Jin, Y.; Zhu, B.; Lu, Z.; Liu, N.; Zhu, J. Challenges and Recent Progress in the Development of Si Anodes for Lithium-Ion Battery. *Adv. Energy Mater.* **2017**, *7* (23), 1700715.

(15) Zheng, J.; Ye, Y.; Liu, T.; Xiao, Y.; Wang, C.; Wang, F.; Pan, F. Ni/Li Disordering in Layered Transition Metal Oxide: Electrochemical Impact, Origin, and Control. *Acc. Chem. Res.* **2019**, *52* (8), 2201−2209.

(16) Ahmed, S.; Pokle, A.; Schweidler, S.; Beyer, A.; Bianchini, M.; Walther, F.; Mazilkin, A.; Hartmann, P.; Brezesinski, T.; Janek, J.; Volz, K. The Role of Intragranular Nanopores in Capacity Fade of Nickel-Rich Layered $Li(Ni_{1-x-y}Co_xMn_y)O_2$ Cathode Materials. *ACS Nano* **2019**, *13* (9), 10694−10704.

(17) Kim, U.-H.; Myung, S.-T.; Yoon, C. S.; Sun, Y.-K. Extending the Battery Life Using an Al-Doped $Li[Ni_{0.76}Co_{0.09}Mn_{0.15}]O_2$ Cathode with Concentration Gradients for Lithium Ion Batteries. *ACS Energy Lett.* **2017**, *2* (8), 1848−1854.

(18) Zeng, X. Q.; Zhan, C.; Lu, J.; Amine, K. Stabilization of a High-Capacity and High-Power Nickel-Based Cathode for Li-Ion Batteries. *Chem.* **2018**, *4* (4), 690−704.

(19) Kim, J.; Ma, H.; Cha, H.; Lee, H.; Sung, J.; Seo, M.; Oh, P.; Park, M.; Cho, J. A highly stabilized nickel-rich cathode material by nanoscale epitaxy control for high-energy lithium-ion batteries. *Energy Environ. Sci.* **2018**, *11* (6), 1449−1459.

(20) Kim, J.; Lee, J.; Ma, H.; Jeong, H. Y.; Cha, H.; Lee, H.; Yoo, Y.; Park, M.; Cho, J. Controllable Solid Electrolyte Interphase in Nickel-Rich Cathodes by an Electrochemical Rearrangement for Stable Lithium-Ion Batteries. *Adv. Mater.* **2018**, *30* (5), 1704309.

(21) Weigel, T.; Schipper, F.; Erickson, E. M.; Susai, F. A.; Markovsky, B.; Aurbach, D. Structural and Electrochemical Aspects of $LiNi_{0.8}Co_{0.1}Mn_{0.1}O_2$ Cathode Materials Doped by Various Cations. *ACS Energy Lett.* **2019**, *4* (2), 508−516.

(22) Sun, Y. M.; Lee, H. W.; Seh, Z. W.; Liu, N.; Sun, J.; Li, Y. Z.; Cui, Y. High-capacity battery cathode prelithiation to offset initial lithium loss. *Nat. Energy* **2016**, *1*, 15008.

(23) Kim, H. J.; Choi, S.; Lee, S. J.; Seo, M. W.; Lee, J. G.; Deniz, E.; Lee, Y. J.; Kim, E. K.; Choi, J. W. Controlled Prelithiation of Silicon Monoxide for High Performance Lithium-Ion Rechargeable Full Cells. *Nano Lett.* **2016**, *16* (1), 282−288.

(24) Zhu, Z.; Yu, D.; Yang, Y.; Su, C.; Huang, Y.; Dong, Y.; Waluyo, I.; Wang, B.; Hunt, A.; Yao, X.; Lee, J.; Xue, W.; Li, J. Gradient Li-rich oxide cathode particles immunized against oxygen release by a molten salt treatment. *Nat. Energy* **2019**, *4* (12), 1049−1058.

(25) Han, J.-G.; Lee, J. B.; Cha, A.; Lee, T. K.; Cho, W.; Chae, S.; Kang, S. J.; Kwak, S. K.; Cho, J.; Hong, S. Y.; Choi, N.-S. Unsymmetrical fluorinated malonatoborate as an amphoteric additive for high-energy-density lithium-ion batteries. *Energy Environ. Sci.* **2018**, *11* (6), 1552−1562.

(26) Maiti, S.; Sclar, H.; Rosy; Grinblat, J.; Talianker, M.; Burstein, L.; Noked, M.; Markovsky, B.; Aurbach, D. Modification of Li- and Mn-Rich Cathode Materials via Formation of the Rock-Salt and Spinel Surface Layers for Steady and High-Rate Electrochemical Performances. *ACS Appl. Mater. Interfaces* **2020**, *12* (29), 32698−32711.

(27) Maleki Kheimeh Sari, H.; Li, X. Controllable Cathode−Electrolyte Interface of $Li[Ni_{0.8}Co_{0.1}Mn_{0.1}]O_2$ for Lithium Ion Batteries: A Review. *Adv. Energy Mater.* **2019**, *9* (39), 1901597.

(28) Wu, Z.; Ji, S.; Zheng, J.; Hu, Z.; Xiao, S.; Wei, Y.; Zhuo, Z.; Lin, Y.; Yang, W.; Xu, K.; Amine, K.; Pan, F. Prelithiation Activates $Li(Ni_{0.5}Mn_{0.3}Co_{0.2})O_2$ for High Capacity and Excellent Cycling Stability. *Nano Lett.* **2015**, *15* (8), 5590−5596.

(29) Sun, G.; Yu, F. D.; Que, L. F.; Deng, L.; Wang, M. J.; Jiang, Y. S.; Shao, G. J.; Wang, Z. B. Local electronic structure modulation enhances operating voltage in Li-rich cathodes. *Nano Energy* **2019**, *66*, 104102.

(30) Wang, D. W.; Xin, C.; Zhang, M. J.; Bai, J. M.; Zheng, J. X.; Kou, R. H.; Ko, J. Y. P.; Huq, A.; Zhong, G. M.; Sun, C. J.; Yang, Y.; Chen, Z. H.; Xiao, Y. G.; Amine, K.; Pan, F.; Wang, F. Intrinsic Role of Cationic Substitution in Tuning Li/Ni Mixing in High-Ni Layered Oxides. *Chem. Mater.* **2019**, *31* (8), 2731−2740.
(31) Zhang, M. J.; Teng, G.; Chen-Wiegart, Y. K.; Duan, Y.; Ko, J. Y. P.; Zheng, J.; Thieme, J.; Dooryhee, E.; Chen, Z.; Bai, J.; Amine, K.; Pan, F.; Wang, F. Cationic Ordering Coupled to Reconstruction of Basic Building Units during Synthesis of High-Ni Layered Oxides. *J. Am. Chem. Soc.* **2018**, *140* (39), 12484−12492.
(32) Wang, R.; Qian, G.; Liu, T.; Li, M.; Liu, J.; Zhang, B.; Zhu, W.; Li, S.; Zhao, W.; Yang, W.; Ma, X.; Fu, Z.; Liu, Y.; Yang, J.; Jin, L.; Xiao, Y.; Pan, F. Tuning Li-enrichment in high-Ni layered oxide cathodes to optimize electrochemical performance for Li-ion battery. *Nano Energy* **2019**, *62*, 709−717.
(33) Tang, Z.; Wang, S.; Liao, J.; Wang, S.; He, X.; Pan, B.; He, H.; Chen, C. Facilitating Lithium-Ion Diffusion in Layered Cathode Materials by Introducing Li^{+}/Ni^{2+} Antisite Defects for High-Rate Li-Ion Batteries. *Research* **2019**, *2019*, 2198906.
(34) Liu, X.; Tan, Y.; Wang, W.; Li, C.; Seh, Z. W.; Wang, L.; Sun, Y. Conformal Prelithiation Nanoshell on $LiCoO_2$ Enabling High-Energy Lithium-Ion Batteries. *Nano Lett.* **2020**, *20* (6), 4558−4565.
(35) Liu, X.; Tan, Y.; Liu, T.; Wang, W.; Li, C.; Lu, J.; Sun, Y. A Simple Electrode-Level Chemical Presodiation Route by Solution Spraying to Improve the Energy Density of Sodium-Ion Batteries. *Adv. Funct. Mater.* **2019**, *29* (50), 1903795.
(36) Shen, Y.; Zhang, J.; Pu, Y.; Wang, H.; Wang, B.; Qian, J.; Cao, Y.; Zhong, F.; Ai, X.; Yang, H. Effective Chemical Prelithiation Strategy for Building a Silicon/Sulfur Li-Ion Battery. *ACS Energy Lett.* **2019**, *4* (7), 1717−1724.
(37) Johnson, C. S.; Kim, J.-S.; Kropf, A. J.; Kahaian, A. J.; Vaughey, J. T.; Fransson, L. M. L.; Edström, K.; Thackeray, M. M. Structural Characterization of Layered $Li_xNi_{0.5}Mn_{0.5}O_2$ ($0 < x \leq 2$) Oxide Electrodes for Li Batteries. *Chem. Mater.* **2003**, *15* (12), 2313−2322.
(38) Kong, D.; Zhang, M.; Xiao, Y.; Hu, J.; Zhao, W.; Han, L.; Pan, F. Insights into the structural evolution and Li/O loss in high-Ni layered oxide cathodes. *Nano Energy* **2019**, *59*, 327−335.
(39) Kim, Y.; Kim, D.; Kang, S. Experimental and First-Principles Thermodynamic Study of the Formation and Effects of Vacancies in Layered Lithium Nickel Cobalt Oxides. *Chem. Mater.* **2011**, *23* (24), 5388−5397.
(40) Myeong, S.; Cho, W.; Jin, W.; Hwang, J.; Yoon, M.; Yoo, Y.; Nam, G.; Jang, H.; Han, J. G.; Choi, N. S.; Kim, M. G.; Cho, J. Understanding voltage decay in lithium-excess layered cathode materials through oxygen-centred structural arrangement. *Nat. Commun.* **2018**, *9* (1), 3285.
(41) Qiu, B.; Zhang, M.; Xia, Y.; Liu, Z.; Meng, Y. S. Understanding and Controlling Anionic Electrochemical Activity in High-Capacity Oxides for Next Generation Li-Ion Batteries. *Chem. Mater.* **2017**, *29* (3), 908−915.
(42) Cho, Y.; Oh, P.; Cho, J. A new type of protective surface layer for high-capacity Ni-based cathode materials: nanoscaled surface pillaring layer. *Nano Lett.* **2013**, *13* (3), 1145−1152.
(43) Myung, S.-T.; Maglia, F.; Park, K.-J.; Yoon, C. S.; Lamp, P.; Kim, S.-J.; Sun, Y.-K. Nickel-Rich Layered Cathode Materials for Automotive Lithium-Ion Batteries: Achievements and Perspectives. *ACS Energy Lett.* **2017**, *2* (1), 196−223.
(44) Xiao, Y.; Liu, T.; Liu, J.; He, L.; Chen, J.; Zhang, J.; Luo, P.; Lu, H.; Wang, R.; Zhu, W.; Hu, Z.; Teng, G.; Xin, C.; Zheng, J.; Liang, T.; Wang, F.; Chen, Y.; Huang, Q.; Pan, F.; Chen, H. Insight into the origin of lithium/nickel ions exchange in layered $Li(Ni_xMn_yCo_z)O_2$ cathode materials. *Nano Energy* **2018**, *49*, 77−85.

https://dx.doi.org/10.1021/acsenergylett.0c02487
ACS Energy Lett. 2021, 6, 320−328